Extending Near Field Communication Range for Ultra-Dense Internet of Things

Omar Ansari and Hongzhi Guo, *Senior Member, IEEE*

***Abstract*—The advent of 6G wireless systems promises a digital world that blends physical and virtual elements, revolutionizing our interaction with the physical environment. A critical step towards this digital world is the creation of digital twins of physical systems and objects. The Internet of Things (IoT) plays an important role in connecting and monitoring these physical entities. However, connecting all objects in our daily life is challenging due to high density and large number of devices. Near Field Communication (NFC), utilizing High Frequency (HF) band signals, emerges as a promising solution. NFC has a short communication range and high penetration efficiency, with a reliable wireless channel that does not compete for spectrum with typical cellular and local area networks. Nevertheless, its extremely short range limits its use in autonomous IoT applications. This paper explores two techniques to extend NFC's communication range and reliability: the use of high-quality factor transmit/receive coils and high-quality factor relay coils. Additionally, the effect of tag coil coupling in a multi-tag IoT environment is examined. Analytical models are developed to evaluate these approaches, and the results are validated using COMSOL Multiphysics. The findings demonstrate a significant increase in NFC's communication range, i.e., up to 0.9 – 1.3 m for 1 – 10 W transmit power, making it suitable for ultra-dense battery-free IoT operations.**

***Index Terms*—Communication range, high Q coils, near field communication, ultra-dense IoT.**

I. Introduction

6G wireless systems are set to revolutionize wireless communication by leveraging the entire electromagnetic spectrum and providing global coverage. A key driving force behind 6G is the digitalization of the physical world, enabling the creation of virtual content and fostering the development of metaverse and extended reality (XR) technologies [1]. The metaverse will offer hyper-real virtual content, providing experiences that are either impossible or inaccessible in the physical world. Extended reality, encompassing virtual reality (VR), mixed reality (MR), and augmented reality (AR), will serve as gateways to the metaverse. To construct this virtual world, it is essential to create digital twins of physical objects and systems, while connecting them through Internet of Things (IoT) technologies.

The success of Chat-GPT has proven that Artificial Intelligence (AI) can significantly change our daily lives. However, we can only ask questions which can be answered based on existing knowledge. It remains challenging to get suggestions from AI on real-time activities or personal life. This is due to the lack of IoT technologies which can synchronize everything in the physical world with that in the virtual/digital world.

The large number and high density of everyday things make the design of IoT challenging. Battery-powered IoT solutions are not suitable since they require maintenance and usually use bulky devices. As a result, they mainly support data-intensive wireless applications. Battery-free IoT solutions using Radio-Frequency IDentification (RFID), Ambient Backscatter Communication (AmBC), and Near Field Communication (NFC) are promising due to their low-cost and tiny size of tags/devices which can be easily attached to everyday things.

Ultra High Frequency (UHF) RFID has been widely adopted in IoT, e.g., clothes are tagged for tracking in the process of manufacturing and sales. However, it is not suitable for ultra-dense IoT for everyday use due to the following five reasons. First, due to multipath fading, noise, interference, and other random effects, UHF RFID has blind areas, where tags cannot be read [2], [3]. Second, the ISM band at 915 MHz is widely used by many other applications, such as LoRa [4], Zigbee [5], and industrial radios (e.g., MDS TransNET [6] which is used for oil metering station). The UHF RFID may interfere with these radios due to its long communication range. Third, the UHF RFID impedance can be changed by the attached object and surrounding environment, which affects its performance [7], [8]. Also, the penetration efficiency of UHF signals is low, which cannot efficiently penetrate through high-permittivity and high-conductivity materials. Finally, the long communication range of UHF RFID makes it more susceptible to attacks by unauthorized users and it is challenging to achieve high-level security. Due to these reasons, UHF RFID is suitable for low-density applications only, where tags are well-separated and powerful readers are available.

AmBC shares the same foundation as the UHF RFID, but it is low-cost and power-efficient because it does not use a dedicated reader [9]–[11]. Since it backscatters WiFi, LTE, mmWave, and LoRa signals, its performance is affected by the legacy networks. Usually, the receiver must be close to the transmitter in order to receive high-quality signals. For ultra-dense IoT, AmBC may experience delay, misreading, and significant packet losses. It cannot meet the expected requirements.

NFC uses the High Frequency (HF) band at 13.56 MHz and HF signals demonstrate several advantages over UHF signal. First, this band does not compete for spectrum with other IoT technologies operating at UHF band. Second, the short range and inverse cube dependence of magnetic field on distance

O. Ansari and H. Guo are with the School of Computing at University of Nebraska-Lincoln, Lincoln, NE, 68588, USA. Emails: hansari2@unl.edu and hguo10@unl.edu.

This work is supported by National Science Foundation under grant No. CNS-2310856

make the HF NFC design immune to external interference and attacks. Another kind of interference can be due to closely placed multiple tags. This aspect is important when it comes to interference in IoT for ultra-dense environments. We have discussed this issue in our paper. Third, it has a long wavelength which can easily penetrate non-magnetic materials, making NFC ideal for IoT applications.

Along with all the promising prospects, these are also several challenges associated with NFC. NFC has an extremely short communication range which cannot support autonomous networking and users must manually scan NFC tags/sensors. For large scale autonomous IoT, we need to extend current NFC's range by at least 10 times. Existing works have explored various ways to extend NFC's range using coil arrays, magnetic beamforming, repeaters/relays, and signal processing techniques [12]–[15]. The separated transmitter and receiver design is proposed in [13] where the transmitter and receiver operate at different frequencies to allow the adoption of high Quality factor (Q) coils. In [16], an over-coupling topology has been introduced that relies on using high Q coils to extend the tag read range. The drawback of using high Q coils, however, is its adverse effect on bandwidth or capacity. Another challenge associated with the design of high Q coils is their fabrication variability. It is difficult to design high Q coils for narrow-band operation due to process variations. The performance of high Q coils is affected by the surrounding environment. For instance, if there are metallic objects surrounding the coil, a significant shift in resonance frequency can be observed. However, with the intelligent use of adaptive circuits, the effects of these issues can be mitigated. For high data rate applications, orbital angular momentum based NFC has been proposed [17]. The authors present a review of NFC technology and its potential for integration with wearable devices in an ultra-dense setting for continuous monitoring and medical applications in [18].

The extended range of HF NFC systems has significant practical implications in terms of its potential applications. The use of NFC technology in IoT industry is only limited due to short communication range of current NFC systems. With extended range, tags coils can be deployed for sensing and tracking of everyday items in different environments and settings. Some of the potential applications are digital twins [19], IoT-enabled robotics and smart homes [20], augmented reality [21], bio-medical healthcare applications [22], and logistics/asset tracking [23].

In our paper, we combine the range enhancing capabilities of high Q coils and relay coils, and develop analytical models to study the advantages of each approach. We use separated transmitter and receiver in NFC readers and use high Q coils as in [13]. However, we use a relatively small transmitter and receiver which can be deployed on mobile robots. Also, we optimize the tag coil's and relay coil's resonant frequencies and quality factors to further increase the communication range. Also, we study the impact of tag coil coupling to show its negative impact on extending communication range. The developed analytical model can be utilized as a guideline for long-range NFC design and optimization.

The rest of this paper is organized as follows. In Section II, we introduce the international standards for mid-range and long-range NFC. In Section III, we present the NFC system model and explore the mechanisms for range extension using various coils. The impact of tag coil coupling in ultra-dense IoT environment is also discussed. After that, we discuss simulation results in Section IV. Finally, this paper is concluded in Section V.

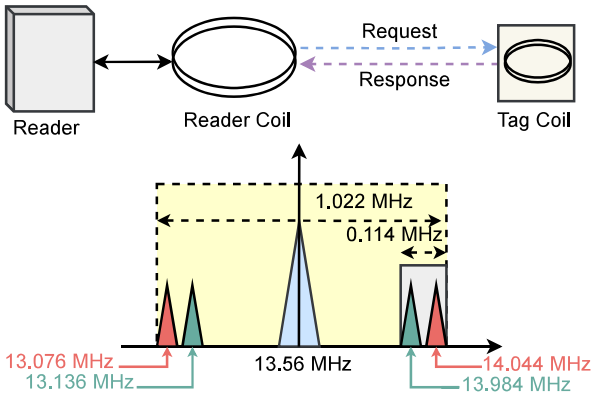

Fig. 1: Illustration of ISO/IEC15693 communication system. An example of the spectrum is given in the lower part.

II. Long-range NFC Standards

Existing NFC coils normally have a quality factor of 8. This is due to the fact that a single NFC coil needs to support multiple NFC standards with different bandwidths and data rates. ISO/IEC14443 supports the high data rate of 848 kbps with a subcarrier frequency of 848 kHz [24]. Therefore, the quality factor must be selected to enable a minimum bandwidth of 1.696 MHz, which corresponds to $Q = 13.56/1.696 \approx 8$.

Since the data rates of ISO/IEC15693 [25] are lower than that of ISO/IEC14443, the bandwidth of coils with $Q = 8$ is more than sufficient. The communication from reader to tag uses 13.56 MHz as the carrier frequency and supports two different data rates. There are two subcarrier frequency options for reader to tag communication. First, it can use a single subcarrier frequency at 423.75 kHz with data rates of 6.62 kbps or 26.48 kbps. Second, it can use double subcarrier frequencies at 423.75 kHz and 484.28 kHz. The achievable data rates are 6.67 kbps and 26.69 kbps. As shown in Fig. 1, the overall bandwidth is around 1.022 MHz if we use one coil for receiving and transmitting, which corresponds to $Q = 13.56/1.022 \approx 13$. Therefore, ISO/IEC15693 allows stronger coupling between the reader coil and the tag coil using larger coil quality factor. As a result, the communication range is longer.

Besides the constraint of quality factor, there are also constraints on the minimum and maximum operating magnetic fields. The minimum operating magnetic field h_{min} for ISO/IEC15693 is 150 mA/m rms, which is to ensure that the signal strength at the tag is strong enough for load

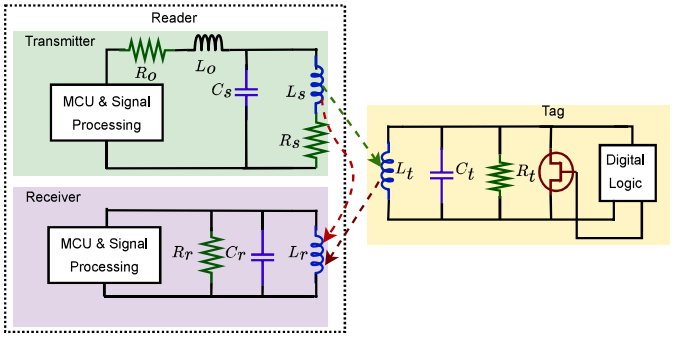

Fig. 2: Equivalent circuit model of the modified NFC system with separated transmitter and receiver circuits in a reader.

modulation. Moreover, the maximum operating magnetic field h_{max} for ISO/IEC15693 is 5 A/m rms for safety concerns. Although using a high transmission power can improve the communication range, the constraint of maximum magnetic field strength limits the maximum transmission power.

III. NFC System Modeling

In this section, we first develop system models for the major components in the NFC system with separated transmitter and receiver. Then, we discuss the impact of ultra-dense tag coil coupling. The relationship between distance, and quality factor for different communication system configurations is also analyzed.

A. Transmitter and Receiver

In this subsection, we develop power and channel models for the separated transmitter and receiver in the NFC reader. The parameters of mutual inductance, self-inductance, bandwidth, and quality factor are jointly considered.

The quality factor of a coil is determined by its inductance and circuit resistance. The self-inductance of a coil L_s with wire radius w_s, coil radius r_s, and n_s number of turns can be written as

$$L_s = \mu_0 n_s^2 r_s \left[\ln\left(\frac{8r_s}{w_s}\right) - 2\right], \tag{1}$$

where μ_0 is the permeability constant in Eqn. (1). The resistance of NFC coil consists of two parts. First, there is coil resistance which is due to the wire conductance and, second, the radiation resistance. Coil resistance is generally very small for thick wires and it can be neglected. The radiation resistance is

$$R_l = \eta\left(\frac{2\pi}{3}\right)\left(\frac{k\pi r_s^2}{\lambda}\right)^2 n_s^2, \tag{2}$$

where $\eta = 120\pi$ is the wave impedance, $k = 2\pi f\sqrt{\mu\epsilon}$ is the propagation constant, $\lambda = 2\pi/k$ is the wavelength. Since the coil antenna size is much smaller than the wavelength and most NFC coils use a small number of turns, the magnitude of radiation resistance is relatively small. Therefore, we connect the antenna coil in series with a resistor R_s which is used

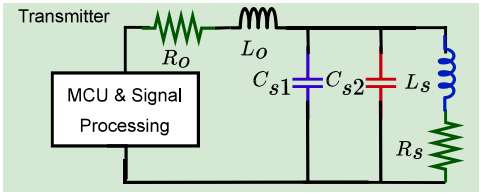

Fig. 3: Equivalent capacitor for impedance matching.

to adjust the quality factor and bandwidth of the circuit. The value of R_s can be adjusted according to the communication requirements. We assume that $R_s = R_l + R_{qt}$, where R_{qt} is a quality factor tuning resistor. The equivalent circuit of the transmitter is shown in Fig. 2, where R_o represents the transmitter resistance, L_o and C_s are the impedance matching inductor and capacitor, respectively. L_s is the source coil inductance.

Given the transmitter resistance R_o, the coil antenna self-inductance L_s, and required quality factor Q_s, we need to find L_o, C_s, and R_s for impedance matching. As shown in Fig. 3, we consider $C_s = C_{s1} + C_{s2}$, where C_{s2} is a virtual capacitor to make the load real. Based on this condition, we can find

$$C_{s2} = \frac{L_s}{\omega^2 L_s^2 + R_s^2}, \tag{3}$$

$$R_{load} = \omega^2 L_s^2 / R_s + R_s. \tag{4}$$

According to [26], the load resistance R_{load} and the transmitter resistance R_o must satisfy

$$\sqrt{R_{load}/R_o - 1} = Q_s. \tag{5}$$

Then, we can obtain

$$R_s = \frac{1 + Q_s^2 - \sqrt{(1+Q_s)^2 - 4\omega^2 L_s^2/R_o}}{2}. \tag{6}$$

Also, we have $L_1 = R_o Q_s/\omega$ and $C_{s1} = Q_s/(\omega R_{load})$. Since R_s is obtained by solving a second order function, there are two possible solutions for it. One of them is valid. The other solution for R_s makes R_{load} larger than R_o, for which the condition of Eqn. (5) becomes invalid. The output voltage signal is $v(t)$ which is considered to have an approximately constant amplitude v_s. Then, the transmission power is $P_s = v_s^2/2R_s$. In other words, given the transmission power, the voltage is $v_s = \sqrt{2P_s R_s}$. The current in the coil i_s can be expressed as

$$i_s = \frac{v_s Z_{s2}}{(Z_{s1} + Z_{s2}) Z_{s3}}, \tag{7}$$

where $Z_{s1} = R_o + j\omega L_o$, $Z_{s3} = j\omega L_s + R_s$, $Z_{s2} = Z_{s3}Z_{s4}/(Z_{s3} + Z_{s4})$, and $Z_{s4} = 1/j\omega C_s$. The magnetic fields generated by the coil in the radial and polar directions can be written as [27]

$$h_r = j\frac{k r_s^2 i_s n_s \cos\theta}{2d^2}\left[1 + \frac{1}{jkd}\right]e^{-jkd}, \tag{8}$$

$$h_\theta = -\frac{(kr_s)^2 i_s n_s \sin\theta}{4d}\left[1 + \frac{1}{jkd} - \frac{1}{(kd)^2}\right]e^{-jkd}. \tag{9}$$

The above equations consider the coils are infinitesimal magnetic dipoles. Since NFC has a short communication range

($kd << 1$) which is much smaller than the wavelength in this case, the far field components in the magnetic field can be ignored and the above equations can be approximated by

$$h_r \approx \frac{r_s^2 i_s n_s \cos\theta}{2d^3}, \quad (10)$$

$$h_\theta \approx \frac{r_s^2 i_s n_s \sin\theta}{4d^3}. \quad (11)$$

The resultant magnetic field from source to tag h_{st} in a spherical coordinates system with location (r, θ, ϕ) can be written as

$$h_{st} = \sqrt{h_r h_r^\dagger + h_\theta h_\theta^\dagger} = \frac{r_s^2 |i_s| n_s}{4d_{st}^3} \sqrt{4\cos^2\theta + \sin^2\theta}, \quad (12)$$

where d_{st} is the distance between the source and tag, $(\cdot)^\dagger$ is the conjugate of a complex number, and $|\cdot|$ is the absolute value of a complex number. Since in the near field, the magnetic fields are mainly real, the conjugate of a magnetic field is itself. As the source and tag coils are coaxial, the angle between them is $\theta = 0^o$. The mutual inductance between them can be calculated as $M_{st} = \mu h_{st} \pi r_t^2 n_t / |i_s| = \mu \pi r_t^2 r_s^2 n_t n_s / 2d_{st}^3$. By replacing the subscript s and t, we can calculate the mutual inductance between any two coils.

The receiver uses a parallel circuit to improve the induced voltage across the load, as shown in Fig. 2. The circuit is resonant at $f_c + f_{sub}$, where f_c and f_{sub} are carrier and subcarrier frequencies, respectively. The angular frequency at the receiver is denoted by $\omega_r = 2\pi(f_c + f_{sub})$. Let $C_r = 1/\omega_r^2 L_r$ and $R_r = \omega_r L_r Q_r$. Then, the induced voltage across R_r is

$$v_r = \left| \frac{\omega_r M_{tr} i_t Z_{r2}}{Z_{r1} + Z_{r2}} \right|, \quad (13)$$

where $Z_{r1} = j\omega_r L_r$, $Z_{r2} = R_r/(j\omega_r C_r(R_r + 1/(j\omega_r C_r)))$, M_{tr} is the mutual inductance between the tag and the receiver coils, and i_r denotes current in the receiver coil.

B. NFC Tag

The minimum magnetic field strength h_{min} is used to guarantee that the induced voltage in the tag is strong enough to power up the tag. However, tags have different coil sizes and require different minimum magnetic field strength. Using a general h_{min} can underestimate the communication range of some NFC systems. In this paper, we use threshold voltage v_{pwr} instead of h_{min} to evaluate the downlink communication range. If the voltage across the tag load in higher than v_{pwr}, we consider the tag can harvest sufficient power to wake up.

The load modulated signal must be demodulated by the receiver. However, the signal must be higher than the receiver's sensitivity voltage, which is considered as a threshold v_{sig}. If the load modulated signal received by the receiver has a voltage lower than v_{sig}, then the receiver cannot demodulate the signal.

We can improve the induced voltage in the tag by increasing its quality factor at 13.56 MHz. However, if the quality factor is significantly large, its efficiency at the center of the two side bands, i.e., $(13.076 + 13.136)/2 = 13.10$ MHz and $(13.984 + 14.044)/2 = 14.01$ MHz will be reduced. On the other hand, we can use one side band to demodulate the signal, e.g., 14.01 MHz, and significantly increase the tag quality factor for this side band. Although this increases the efficiency of transmitted load modulated signal, it reduces the efficiency of power harvesting at 13.56 MHz. Since existing NFC tags use small quality factors and a wide frequency band, the power harvesting efficiency and the tag's load modulation signal transmission have no conflict. As shown in Fig. 1, the transmitter is resonating at 13.56 MHz while the receiver is resonating at 14.01 MHz. Then, we also need to determine the resonant frequency and quality factor of the tag.

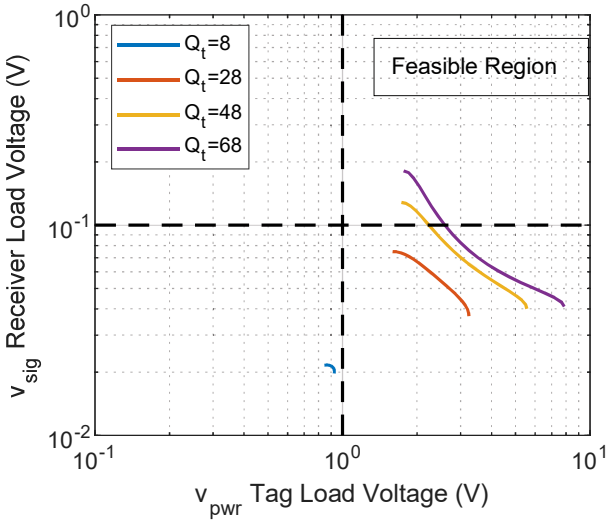

Fig. 4: Feasible region considering the trade-off between v_t and v_r.

First, for power harvesting at 13.56 MHz, the induced voltage in the tag load can be written as

$$v_t = \left| \frac{\omega_s M_{st} i_s Z_{t2}}{Z_{t1} + Z_{t2}} \right|, \quad (14)$$

where $Z_{t1} = j\omega_s L_t$, $Z_{t2} = R_t/(j\omega_s C_t(R_t + 1/(j\omega_s C_t)))$, and M_{st} is the mutual inductance between the source and the tag. In order to wake up the tag, $v_t > v_{pwr}$ must be satisfied. Second, for the load modulated signal transmission, the carrier signal is mixed with a subcarrier signal. Here, we consider the voltage does not drop in the signal mixture process and we have modulated signal with voltage v_t at $f_t = f_c + f_{sub}$. Then, the current in the tag coil is

$$i_t = \left| \frac{\omega_t M_{st} i_s}{\hat{Z}_{t1} + \hat{Z}_{t2}} \right|, \quad (15)$$

where $\hat{Z}_{t1} = j\omega_t L_t$ and $\hat{Z}_{t2} = R_t/(j\omega_t C_t(R_t + 1/(j\omega_t C_t)))$. By replacing i_t in Eqn. (13) using Eqn. (15), we can obtain v_r. In order to meet the receiver sensitivity requirement, $v_r > v_{sig}$ must be satisfied.

In summary, the tag coil circuit design will obtain optimal C_t and R_t (or resonant frequency f_t and quality factor Q_t) to maximize the communication range d under the constraints of $v_t > v_{pwr}$ and $v_r > v_{sig}$.

In Fig. 4, we show the trade-off between v_t and v_r. The transmitter and receiver coils use 10 turns with 0.1 m radius.

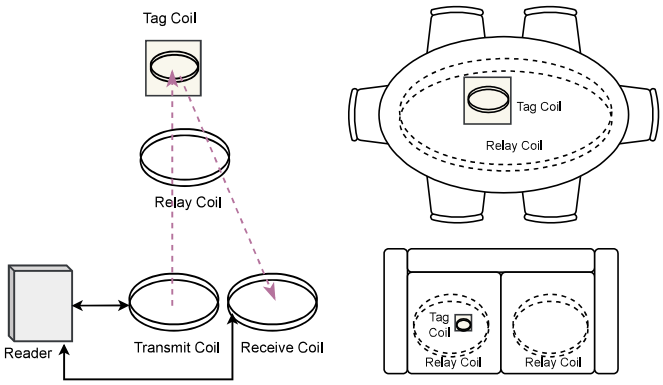

(a) Relay coil (b) Relay coil deployment

Fig. 5: Illustration of relay coil and its placement in daily life applications.

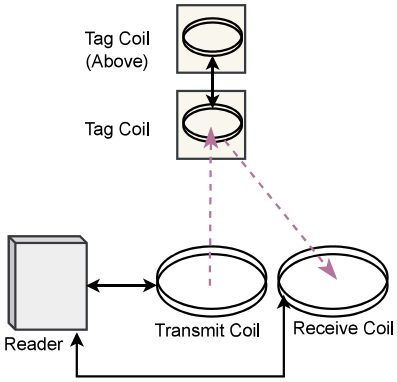

Fig. 6: Tag coil coupling.

The transmission power is 1 W. The quality factor of both coils is 80. The tag coil uses 10 turns with 0.03 m radius. The quality factor of the tag coil is ranging from 8 to 68 with a step of 20. The distance between the tag and the reader is 0.6 m. The resonance frequency of the tag coil is changed from 13.56 MHz to 14.01 MHz and the corresponding v_t and v_r are obtained using Eqn. (13) and Eqn. (14). The threshold voltages are set as $v_{pwr} = 1$V and $v_{sig} = 0.1$ V. As we can see in Fig. 4, when v_t is large, v_r is small, and vice versa. Also, a larger quality factor can generate higher voltages. The feasible region is defined as $v_t > v_{pwr}$ and $v_r > v_{sig}$. If either of the two conditions is not valid, the tag cannot wake up or the receiver cannot demodulate the signal. For example, when the quality factor is 8, there is no feasible solution. The feasible resonance frequency of the tag is determined by the threshold voltages. Note that, the feasible region also depends on the distance between the reader and the tag. When the distance is small, e.g., shorter than 0.05 m, all resonance frequencies between 13.56 MHz and 14.01 MHz can provide feasible v_t and v_r in the existing NFC systems. However, as the distance increases, only large quality factors and certain resonance frequencies can provide feasible solutions.

C. Relay Coil

Due to the fast power fall-off of magnetic signals with respect to distance, increasing transmission power, coil quality factor, and coil radius cannot reach practical communication range for daily life deployment. The application of long-range NFC is mainly IoT, for which we can deploy relay coils in the surrounding environment to further increase the communication range, as shown in Fig. 5. However, the relay coils can only be deployed with certain constraints. For example, they can be deployed on a wall, embedded in a closet, under the table, or inside the cushion.

In practice, relays are deployed at convenient locations and we cannot optimize their locations. The relays can be placed between the reader and the tag or even behind the tag. In this paper, we consider that the relay is arbitrarily placed between the reader and the tag. The relay is a simple series RLC circuit with resonance frequency f_l and quality factor Q_l.

We have derived the expression of tag coil voltage in the presence of a relay coil in Appendix A. In order to provide more insight, we consider a simplified model, where the relay coil voltage is only induced by the transmitter and the tag coil voltage is only induced by the relay coil. This assumption is valid for long range NFC communication as for IoT applications, because as the distance between transmitter and tag increases, the impact of transmitter signal on tag becomes negligible. The transmitter is effectively communicating only to the relay, and an appropriately placed relay is able to send signal to the tag. As a result, $i_l \approx j\omega M_{sl} i_s / R_l$ under resonance condition. Then, we consider the following two cases:

- Using the relay coil, the induced voltage in the tag coil is $|\omega^2 M_{lt} M_{sl} i_s / R_l + \omega M_{st} i_s|$,
- Without using the relay coil, the induced voltage in the tag coil is $|\omega M_{st} i_s|$.

The gain of using relay coil can be approximated by $\frac{\omega M_{lt} M_{sl}}{R_l M_{st}} + 1$. Since both M_{lt} and M_{sl} are much larger than M_{st}, we can design the gain to be much larger than 1 by selecting appropriate R_l.

The derivation of receiver coil voltage in the presence of a relay coil can be found in Appendix B. Similar to the tag coil, there is a trade-off when selecting the relay coil's resonance frequency and quality factor. Since the optimal parameters depend on the receiver's sensitivity, the tag's wake up voltage, and the distance between the reader and the tag which are not constants, the relay coil's resonance frequency is set to $f_l = f_c + f_{sub}/2$ and quality factor is set to 27 so that the relay coil can maintain a bandwidth of f_{sub}.

D. High Density Tags

In an ultra-dense setting, NFC tagged objects can be placed close to each other. When the distance between two tags is short, the tag coils can be strongly coupled and neither of them can communicate. This is due to the strong reflected impedance between coupled coils. There is a minimum separation between two tag coils so that the reader can get sufficient modulated signals from each of the tag.

Consider two tags are closely placed. The current in the tag coil can be modelled as

$$j\omega M_{st} i_s + j\omega M_{tc} i_c + j\omega L_t i_t + R_t i_t/(j\omega C_t R_t + 1) = 0, \tag{16}$$

where i_c is the current in the nearby tag coil and M_{tc} is the mutual inductance between the tag coil and a nearby tag coil. Since the two tag coils are close with the same parameters, thus, their currents must be similar, i.e., $i_c \approx i_t$. Also, the coupling is strong and $M_{tc} \approx L_t$. As a result, the additional coupling between the two tag coils significantly changes the coil current by introducing $j\omega M_{tc} i_c$, which is no longer a negligible factor. However, if the distance between two tag coils is large, this factor is nearly zero. Since it is distance dependent, we cannot use extra capacitors to compensate it.

The significance of the coupling between two tag coils can be evaluated by comparing their mutual inductance with their self-inductance. For this, we can define coupling ratio as

$$\alpha_c = \frac{M_{tc}}{L_t} \approx \frac{\pi}{2\left[\ln\left(\frac{8r_t}{w_i}\right) - 2\right]} \left(\frac{r_t}{d_{tc}}\right)^3, \tag{17}$$

where d_{tc} is the distance between the two tag coils. Also, we implicitly assume the two tag coils have the same radius and number of turns. In order to mitigate the impact of the tag coupling, distance between the two tags must be close to or larger than their coil radius, i.e., $d_{tc} > r_t$.

IV. Numerical Evaluation and Simulation Results

In this section, numerical results are presented to study the impact of high Q transmit/receive and tag coils, relay coils, and the effect of tag coil coupling on NFC's communication range. The performance is also validated using Finite Element simulation.

A. High Q Transmit and Receive Coils

In this paper, we mainly focus on improving the communication range of NFC for ISO15693 protocol. First, we consider a baseline model where the reader uses two separated coils for transmission and reception. The resonance frequency of the reader coil and tag coil is 13.56 MHz. The quality factor of the tag coil is 8. Each coil's radius is 0.0386 m with 5 turns. The coil wire radius is 2 mm. The tag generates a subcarrier signal of frequency 0.45 MHz. We assume the self-interference between the transmit coil and the receive coil can be perfectly cancelled. We also assume that the transmit coil and receive coil are coaxial with the same location. The tag coil is coaxial with the transmit/receive coil and we do not consider coil misalignment in this paper. As a result, the setup is comparable to existing NFC systems.

In Fig. 7, the quality factors of the transmit and receive coils are the same which are varied from 8 to 98 with the step of 30. High quality factor of coil creates narrow bandwidth. Note that, the impact of the transmit coil's high quality factor on communication performance can be improved by using the direct antenna modulation which is not limited by bandwidth [12]. The transmit power is increased from 0.01 W to 10 W.

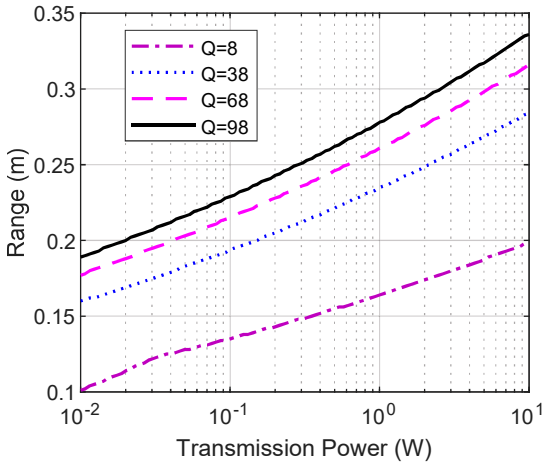

Fig. 7: NFC communication range with different transmit and receive coil quality factors (Q).

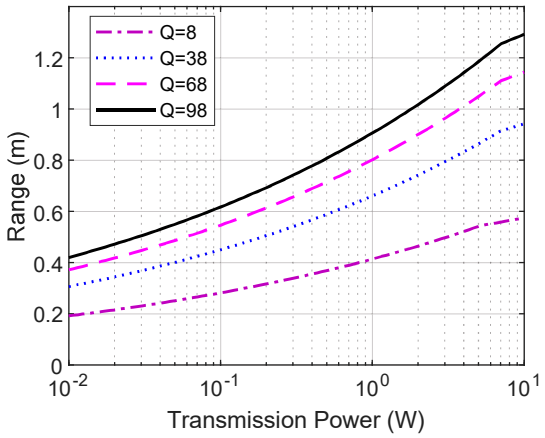

Fig. 8: Impacts of coil quality factor on NFC communication range with a high Q tag coil.

The tag's wake up voltage is $v_{pwr} = 1$ V and the receiver sensitivity voltage is $v_{sig} = 0.1$ V. As we can see from the figure, using a 0.01 W transmit power, the communication range is 0.1 m which is similar to most of the existing NFC systems. As the transmit power increases, the coils with quality factors of 8 can only achieve a 0.2 m communication range even with 10 W transmit power. Note that, existing NFC readers, such as FEIG's long-range NFC reader [28], use transmit power of 8 W, which is comparable to the highest transmit power considered in this paper. If both the transmit and receive coils use a quality factor of 98, we can obtain a communication range of around 0.2 m using 0.01 W transmit power and the maximum communication range increases to 0.34 m.

B. High Q Tag Coil

Although increasing the transmit power and the reader's coil quality factor can increase the communication range, the resonance frequency of the receiver and tag coil can be further optimized as discussed in the previous section. In Fig. 8, the transmit and receive coils' radius is increased from 0.0386 m to 0.1 m. Using large transmit and receive coils is convenient

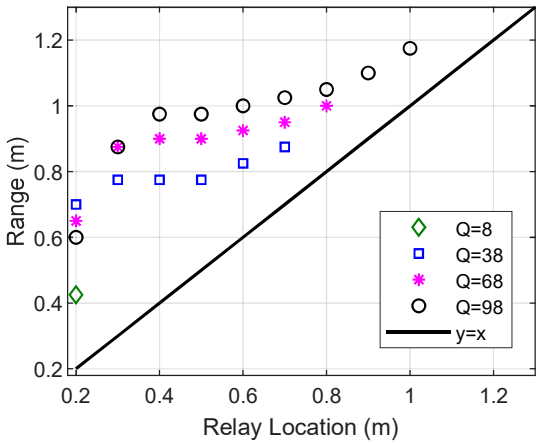

Fig. 9: Impact of relay coil's location on the communication range.

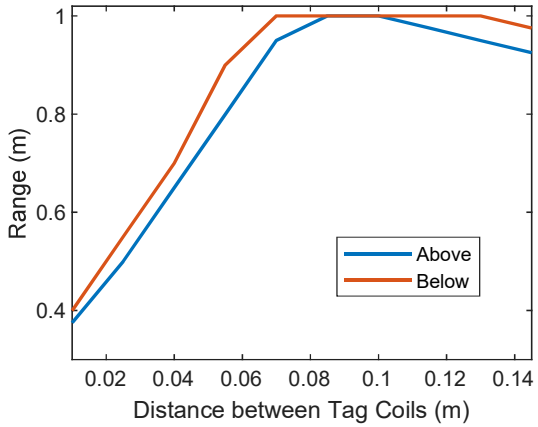

Fig. 10: Impact of tag coil coupling. Blue and red graphs represent the movement of a closely placed tag coil above and below the target tag, respectively.

in IoT and it also contributes towards range enhancement. The number of turns are kept the same equal to 5. The tag coil's radius and number of turns remain 0.0386 m and 5, respectively. The tag coil's quality factor is 48 and resonance frequency is set to 13.79 MHz. The tag's wake up voltage is $v_{pwr} = 1$ V and the receiver sensitivity voltage is $v_{sig} = 0.01$ V. We consider the receiver can use amplifiers to reduce the requirement on v_{sig}. As we can see in the figure, this configuration can improve the communication range to around 1.3 m using transmit and receive coils' quality factor of 98 both and 10 W transmit power. With 1 W transmit power, the range is 0.9 m.

C. Impact of Relay Coil

To evaluate the impact of relay coil, we change the distance between the relay coil and the reader from 0.2 m to 1.2 m. As shown in Fig. 5a, the relay coil is placed above the transmitter and receiver. The tag coil is placed above the relay coil. We also increase the distance between relay coil and tag coil to study the maximum communication range between reader and tag, which is shown in Fig. 9. The transmit power is 1

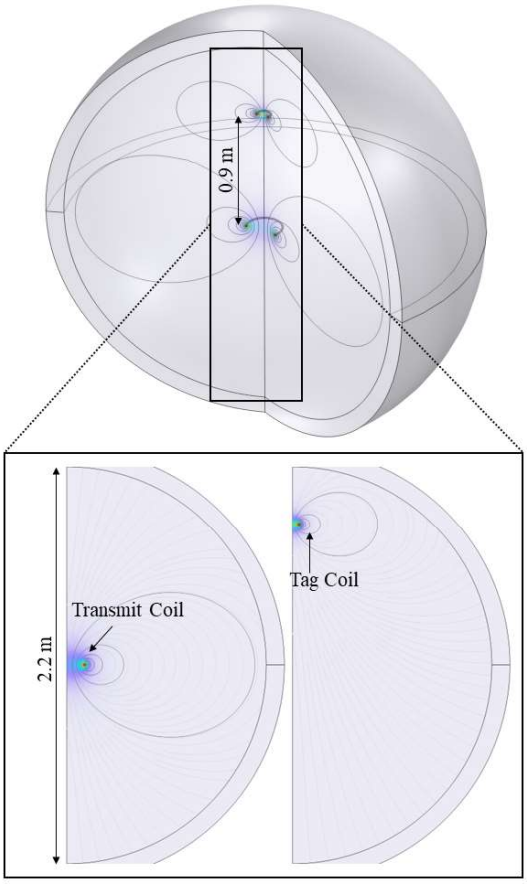

Fig. 11: Finite Element simulation in COMSOL Multiphysics.

W. The relay coil radius is 0.1 m with 5 turns. The quality factor of relay coil is 27 and the resonance frequency is 13.79 MHz, which is the middle of power signal and load-modulated signal. The quality factor of the transmitter/receiver is varied from 8 to 98 with a step size of 30. For example, when the transmitter/receiver quality factor is 8, the relay's distance from the reader is 0.2 m and the communication range is 0.4 m, which means the tag and relay coil's distance is 0.2 m. In Fig. 9, we plot the line $y = x$ which indicates the relay coil's location. The communication range is above $y = x$ and this is because the tag is always above the relay coil, as shown in Fig. 5a. From Fig. 9, we can see that relay coil has significantly improved the communication range compared to the results in Fig. 8. For example, the communication range for quality factor 98 with transmission power 1 W is 0.9 m in Fig. 8, while the range is increased to 1.175 m by placing the relay coil at 1 m distance from the reader. There is no communication range beyond 1 m which means it is impossible to meet the requirements of v_{pwr} and v_{sig} if the relay coil is placed more than 1 m away from the reader.

D. Tag Coil Coupling in Ultra-Dense IoT

In Fig. 6, a tag is placed above another tag. We consider the lower one is the target tag which is used to evaluate the communication range and the higher one is a coupling tag which is used to generate coupling effect. The coupling

TABLE I: Comparison of our work with existing protocols and systems

Ref No.	Protocol / Design	Hardware Complexity	Quality Factor	Transmit Power (W)	Range (m)	Applications
[24]	ISO/IEC14443	Low	Q = 8	P_t = –	0.04 – 0.1	Passive NFC tags reading for very short range applications
[25]	ISO/IEC15693	Low	Q = 13	P_t = –	0.1	Short range passive NFC tags reading
[29]	FEIG's ID LR(M)5400	High	Q = –	$P_t = 1 - 8$	2.0	Designed for logistics tagging and handling, library management, and industrial applications
This work	High Q Tx/Rx and tag coils, relay coil	Normal	Q = 98	$P_t = 1 - 10$	0.9 – 1.3	Tagging in ultra-dense internet of things is the intended application

tag can also be placed below the target tag. In Fig. 10, we show the impact of coupling tag when it is above and below the target tag. The distance between coupling tag and target tag is varied from 0.01 m to 0.1 m. The two tags have the same configuration as before. The transmit power is 1 W. In Fig. 8, the communication range using quality factor 98 and transmission power 1 W is around 0.9 m. Here, when the two tags are close, i.e., the distance is shorter than their radius 0.0386 m, the communication range is significantly reduced due to the strong coupling. However, there is also a region where the coupling coil can improve the communication range when their distance is around 1.5 times the radius and α_c is smaller than 0.2. This is because the tag coils' coupling makes the effective antenna aperture larger and stronger signal strength is received overall. As the distance increases further, the impact of coupling tag diminishes and the communication range converges to that of a single tag (without the effect of coupling tag).

E. Validation in COMSOL Multiphysics

We partially validate the system performance using Finite Element simulation in COMSOL Multiphysics. The AC/DC module with axis symmetry simulation environment is used. As shown in Fig. 11, the transmit coil is placed at the center. The circuits and coil parameters are the same as the simulation in Fig. 8 with quality factor of 98 and transmit power of 1 W. In the simulation, the magnetic field at 0.9 m away from the transmitter is 2.86×10^{-8} T, which can be converted to $v_t = 1.48$ V using Eqn. (14). Note that the magnetic field is measured in T in this paper. Then, we create another model to simulate the tag in which the tag coil is placed 0.9 m from the center, as shown in Fig. 11. We measure the magnetic field at the center which is 7.70×10^{-11} T. Using Eqn. (13), we can obtain $v_r = 0.1$ V. Since both v_t and v_r are higher than the associated v_{pwr} and v_{sig}, the communication range of 0.9 m can be achieved.

F. Performance Comparison

In Table I, we have provided a comparison of our work with existing NFC protocols and practical NFC systems available in the market. The devices working on ISO/IEC14443 protocol have a typical range of 0.04 m to up to 0.1 m depending on the transmit power. With a bandwidth of 1.696 MHz, it allows the maximum quality factor of 8. On the other hand, ISO/IEC15693 provides a maximum range of 0.1 m with normal antenna, and up to 13 quality factor of coils with a bandwidth of 1.022 MHz. It can theoretically go up to 1.5 m, but in reality there is no such product commercially available. The hardware complexity of these two protocols is low and their application is restricted only to short distance passive NFC tagging due to their extremely short range.

For fair comparison, we selected a commercially available FEIG's module ID LR(M)5400 with extended range. However, it is designed for different intended application of logistics, library, and industrial management [29]. It provides a maximum range of 2 m with adjustable transmit power of 1 W to 8 W. The complexity of device is relatively high as it comprises of multiple RF ports and antennas. The technique proposed in our paper can provide up to 0.9 m range with high quality factor of 98 and 1 W transmit power, making it ideal for IoT applications. Note that we can also achieve the range of 1.3 m with increased transmit power of 10 W, as shown in Section III (B). The hardware complexity of our design is normal as it does not require multiple Tx/Rx ports. It just relies on taking the advantage of high Q coils.

V. Conclusion

In this paper, we analyzed two approaches for extending the range of existing NFC for ultra-dense IoT applications. First, the use of high Q coils including transmit, receive, and tag coils. Second, relay coils that are embedded in the environment are used to extend the communication range. We also presented the effect of mutual coupling in tags due to their close vicinity in ultra-dense IoT scenarios. Results suggest that the distance between two tags must be close to or greater than the tag coil radius. It is shown that by using high Q transmit/receive and tag coils, and with the introduction of relay coil, the communication range of existing NFC systems can be significantly enhanced to 0.9 – 1.3 m for transmit power ranging from 1 W to 10 W. This makes HF NFC an attractive tagging and identification solution for IoT technologies.

Appendix

A. Derivation of Tag Coil Voltage in the Presence of a Relay Coil

In previous analysis, we considered that the transmitter/receiver coil and the tag coil are loosely coupled, i.e., the reflected impedance is not considered. This approximation is effective when the communication range is larger than the coil size. However, the relay coil is close to the tag coil and its size can be much larger than the distance between the two coils. Thus, it is not effective to consider they are loosely

coupled. Therefore, we use the exact analysis based on the circuit model in Fig. 2 and the illustration in Fig. 5a. We can obtain the following equations

$$i_o - i_{sc} - i_s = 0 \tag{18}$$

$$R_o i_o + j\omega L_o i_o + i_{sc}/j\omega C_s = v_s \tag{19}$$

$$R_o i_o + j\omega L_o i_o + j\omega L_s i_s + R_s i_s + j\omega M_{st} i_t + j\omega M_{sl} i_l = v_s \tag{20}$$

$$j\omega M_{sl} i_s + R_l i_l + (j\omega L_l + 1/(j\omega C_l))i_l + j\omega M_{lt} i_t = 0 \tag{21}$$

$$j\omega M_{st} i_s + j\omega M_{lt} i_l + j\omega L_t i_t + R_t i_t/(j\omega C_t R_t + 1) = 0, \tag{22}$$

where i_o is the current in R_o, i_{sc} is the current in C_s, i_s is the current in the transmit coil L_s, i_l is the current in the relay coil with resistance R_l, coil self-inductance is L_l, tuning capacitance is C_l, and i_t is the current in the tag coil. The receiver is not included in this problem since its impact on the relay coil and tag coil is negligible due to its small current. The above equations have five unknown current parameters, i.e., i_o, i_{sc}, i_s, i_t, and i_l. Since we have five equations, the unknown parameters can be found by solving the linear equations. Moreover, since the relay coil can be much larger than the tag coil, the mutual inductance approximation is not accurate. According to [30], the accurate mutual inductance between a coaxial coil 1 and a coil 2 can be written as

$$M_{21} = \mu_0 \pi n_1 n_2 r_1 r_2 \int_0^\infty J_0(sp) J_1(sr_2) J_1(sr_1) \exp(-s|z_2 - z_1|)\, ds, \tag{23}$$

where p is the perpendicular distance separating the coil axes, $|z_2 - z_1|$ is the vertical distance separating the coil planes, $J_n(\cdot)$ is the n^{th} order Bessel function, n_i (i={1,2}) is the number of turns of coil, and r_i (i={1,2}) is coil radius, and s is the variable of integration. Then, the voltage of the tag load is

$$v_t = |i_t Z_{t2}|. \tag{24}$$

B. Derivation of Receiver Coil Voltage in the Presence of a Relay Coil

The tag performs load modulation by using subcarrier signals and we assume the mixed signal amplitude is the same as the carrier signal. Since the transmitter and the receiver have different resonant frequencies, we only use the relay, tag, and receiver circuits to obtain the receiver current. The equations can be expressed as

$$R_l \hat{i}_l + (j\omega_s L_l + 1/(j\omega_s C_l))\hat{i}_l + j\omega_s M_{lt} \hat{i}_t = 0 \tag{25}$$

$$j\omega M_{st} i_s + j\omega M_{lt} i_l + j\omega_s L_t \hat{i}_t + R_t \hat{i}_t/(j\omega C_t R_t + 1) + j\omega_s M_{lt} \hat{i}_l = 0 \tag{26}$$

$$j\omega_s M_{tr} \hat{i}_t + j\omega_s M_{lr} \hat{i}_l + (Z_{r1} + Z_{r2})\hat{i}_r = 0, \tag{27}$$

The i_s and i_l are obtained from Eqn. (18) to Eqn. (22). Using the above three equations, we can obtain the currents of the tag $\hat{i}_t$, relay $\hat{i}_l$, and receiver $\hat{i}_r$. The induced voltage in the receiver coil is

$$v_r = |\hat{i}_r Z_{r2}|. \tag{28}$$

REFERENCES

[1] I. F. Akyildiz and H. Guo, "Holographic-type communication: A new challenge for the next decade," *ITU Journal on Future and Evolving Technologies.*, vol. 3, no. 2, pp. 421–442, 2022.

[2] C. Loo, A. Elsherbeni, F. Yang, and D. Kajfez, "Experimental and simulation investigation of rfid blind spots," *Journal of Electromagnetic Waves and Applications*, vol. 23, no. 5-6, pp. 747–760, 2009.

[3] Y. Wang and X. Xu, "Indoor localization service based on the data fusion of wi-fi and rfid," in *2016 IEEE International Conference on Web Services (ICWS)*. IEEE, 2016, pp. 180–187.

[4] M. C. Bor, U. Roedig, T. Voigt, and J. M. Alonso, "Do lora low-power wide-area networks scale?" in *Proceedings of the 19th ACM International Conference on Modeling, Analysis and Simulation of Wireless and Mobile Systems*, 2016, pp. 59–67.

[5] H. Zemrane, Y. Baddi, and A. Hasbi, "Comparison between iot protocols: Zigbee and wifi using the opnet simulator," in *Proceedings of the 12th International Conference on Intelligent Systems: Theories and Applications*, 2018, pp. 1–6.

[6] "MDS TransNET," available: https://www.solidsignal.com.

[7] P. Sen, S. N. R. Kantareddy, R. Bhattacharyya, S. E. Sarma, and J. E. Siegel, "Low-cost diaper wetness detection using hydrogel-based rfid tags," *IEEE Sensors Journal*, vol. 20, no. 6, pp. 3293–3302, 2019.

[8] M. Škiljo, P. Šolić, Z. Blažević, and T. Perković, "Analysis of passive rfid applicability in a retail store: What can we expect?" *Sensors*, vol. 20, no. 7, p. 2038, 2020.

[9] V. Liu, A. Parks, V. Talla, S. Gollakota, D. Wetherall, and J. R. Smith, "Ambient backscatter: Wireless communication out of thin air," *ACM SIGCOMM Computer Communication Review*, vol. 43, no. 4, pp. 39–50, 2013.

[10] A. N. Parks, A. Liu, S. Gollakota, and J. R. Smith, "Turbocharging ambient backscatter communication," *ACM SIGCOMM Computer Communication Review*, vol. 44, no. 4, pp. 619–630, 2014.

[11] V. Talla, J. Smith, and S. Gollakota, "Advances and open problems in backscatter networking," *GetMobile: Mobile Computing and Communications*, vol. 24, no. 4, pp. 32–38, 2021.

[12] U. Azad and Y. E. Wang, "Direct antenna modulation (dam) for enhanced capacity performance of near-field communication (nfc) link," *IEEE Transactions on Circuits and Systems I: Regular Papers*, vol. 61, no. 3, pp. 902–910, 2013.

[13] R. Zhao, P. Wang, Y. Ma, P. Zhang, H. H. Liu, X. Lin, X. Zhang, C. Xu, and M. Zhang, "NFC+ breaking nfc networking limits through resonance engineering," in *Proceedings of the Annual conference of the ACM Special Interest Group on Data Communication on the applications, technologies, architectures, and protocols for computer communication*, 2020, pp. 694–707.

[14] J. Jadidian and D. Katabi, "Magnetic mimo: How to charge your phone in your pocket," in *Proceedings of the 20th annual international conference on Mobile computing and networking*, 2014, pp. 495–506.

[15] J. Wang, J. Zhang, K. Li, C. Pan, C. Majidi, and S. Kumar, "Locating everyday objects using nfc textiles," in *Proceedings of the 20th International Conference on Information Processing in Sensor Networks (co-located with CPS-IoT Week 2021)*, 2021, pp. 15–30.

[16] M. Shahmohammadi, M. Chabalko, and A. P. Sample, "High-q, over-coupled tuning for near-field rfid systems," in *2016 IEEE International Conference on RFID (RFID)*, 2016, pp. 1–8.

[17] R. Lyu, W. Cheng, and W. Zhang, "Modeling and performance analysis of oam-nfc systems," *IEEE Transactions on Communications*, vol. 69, no. 12, pp. 7986–8001, 2021.

[18] Z. Cao, P. Chen, Z. Ma, S. Li, X. Gao, R.-x. Wu, L. Pan, and Y. Shi, "Near-field communication sensors," *Sensors*, vol. 19, no. 18, 2019. [Online]. Available: https://www.mdpi.com/1424-8220/19/18/3947

[19] A. R. Al-Ali, R. Gupta, T. Zaman Batool, T. Landolsi, F. Aloul, and A. Al Nabulsi, "Digital twin conceptual model within the context of internet of things," *Future Internet*, vol. 12, no. 10, 2020. [Online]. Available: https://www.mdpi.com/1999-5903/12/10/163

[20] R. Singh, G. Anita, S. Capoor, G. Rana, R. Sharma, and S. Agarwal, *Internet of Things Enabled Robot Based Smart Room Automation and Localization System*. Cham: Springer International Publishing, 2019, pp. 105–133. [Online]. Available: https://doi.org/10.1007/978-3-030-04203-5_6

[21] Y. Park, S. Yun, and K.-H. Kim, "When iot met augmented reality: Visualizing the source of the wireless signal in ar view," in *Proceedings of the 17th Annual International Conference on Mobile Systems, Applications, and Services*, ser. MobiSys '19. New York, NY, USA: Association for Computing Machinery, 2019, p. 117–129. [Online]. Available: https://doi.org/10.1145/3307334.3326079

[22] X. Sun, C. Zhao, H. Li, H. Yu, J. Zhang, H. Qiu, J. Liang, J. Wu, M. Su, Y. Shi, and L. Pan, "Wearable near-field communication sensors for healthcare: Materials, fabrication and application," *Micromachines (Basel)*, vol. 13, no. 5, p. 784, May 2022.
[23] L. Ye, Y. Wang, and J. Chen, "Research on the intelligent warehouse management system based on near field communication (NFC) technology," *Int. J. Adv. Pervasive Ubiquitous Comput.*, vol. 8, no. 2, pp. 38–55, Apr. 2016.
[24] ISO, Geneva, Switzerland, "Identification cards – Contactless integrated circuit cards – Proximity cards," no. ISO 14443, 2016.
[25] ——, "Identification cards – Contactless integrated circuit cards – Vicinity cards," no. ISO 15693, 2006.
[26] M. Steer, *Microwave and RF Design: A Systems Approach*. SciTech Publishing Incorporated, 2009. [Online]. Available: https://books.google.com/books?id=gc7MYgEACAAJ
[27] C. A. Balanis, *Antenna theory: analysis and design*. John wiley & sons, 2015.
[28] FEIG Electronic, "HF Loop Antenna ID ISC.ANT310/310," www.feig.de, Nov. 2016.
[29] FEIG, "Hf long range reader module id lrm5400," FEIG, Tech. Rep., 2024, accessed: 2024-07-22. [Online]. Available: https://www.feig.de/en/products/identification/product/id-lrm5400/
[30] J. T. Conway, "Inductance calculations for noncoaxial coils using bessel functions," *IEEE Transactions on Magnetics*, vol. 43, no. 3, pp. 1023–1034, 2007.

Omar Ansari is a Ph.D. student at the University of Nebraska-Lincoln (UNL), Nebraska, USA, where he serves as a Graduate Research Assistant in the Wireless Intelligent Sensing (WISE) group within the School of Computing. He earned his M.S. degree in Electrical Engineering with highest distinction from the Institute of Space Technology (IST), Islamabad, Pakistan, in 2019, and his B.S. degree in Electrical Engineering from the University of Engineering and Technology (UET), Taxila, Pakistan, in 2015. From April 2019 to April 2024, he worked as a Research Associate at the Cyber & Information Security Lab (CISL) at IST, Islamabad. Prior to that, from 2017 to 2019, he was a Research Assistant at the Wireless Information & Signal Processing (WISP) Lab at IST. He has contributed to several nationally funded projects, including the development of a basic communication system based on Offset Circular Polarization Modulation (OCPM), and the development of High Altitude Platforms (HAP) for backhaul internet connectivity in remote areas. His research interests include secure wireless communication, near-field communication, the Internet of Things (IoT), novel modulation schemes, antenna array design, and RF circuits.

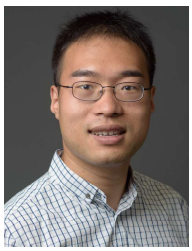

Hongzhi Guo received his Ph.D. degree from the University at Buffalo, the State University of New York in 2017, and his MS degree from Columbia University in 2012, both in Electrical Engineering. Currently, he is an assistant professor in the School of Computing at the University of Nebraska-Lincoln. He was with Norfolk State University and the University of Southern Maine. His research focuses on advancing wireless sensing and communication networks in challenging underground and underwater environments and integrating digital twin and multimodal machine learning techniques to enhance context awareness in complex environments. He received the NSF CAREER award in 2022, the NSF CRII award in 2020, the Jeffress Trust Awards Program in Interdisciplinary Research in 2020, the NSF HBCU-UP RIA award in 2020, and the Best Demo Award in IEEE INFOCOM 2017.